# Stochastic design of high altitude propellers

Adrián García-Gutiérrez[1], Jesús Gonzalo, Deibi López, Adrián Delgado

[a] *Universidad de León, Aerospace Engineering Area, Campus de Vegazana S/n, León, 24071, Spain*

**Abstract**

High-Altitude Platform Stations or High-Altitude Pseudo-Satellites (HAPS) use propulsion systems which are commonly based on propellers. In this paper, an algorithm for the design of those propellers considering uncertainties is developed and applied. The algorithm is based on the non intrusive polynomial chaos expansion scheme, which converts the stochastic design problem into an equivalent deterministic one. Two uncertainties are studied and characterized: 1) the stratospheric wind fluctuations using reanalysis datasets and 2) the variability of the aerodynamic coefficients caused by the low Reynolds number. The results of the method are analyzed to tackle how relevant the uncertainties are in the propulsion of the stratospheric platforms. The case of study is an ideal stratospheric airship that operates at a mean wind speed of 9 m/s and requires a thrust of 100 N, both uncertain magnitudes. The propeller is built on NACA4412 airfoils and the cost function to be maximized is the mean net propulsion efficiency. The new method provides a relevant gain in the mean efficiency when compared with the deterministic optimization.

*Keywords:* stochastic, propeller, optimization

**Nomenclature**

| | |
|---|---|
| $a$ | Sound speed |
| $B$ | Number of blades |

[1] Corresponding author: agarcg@unileon.es

| | |
|---|---|
| B-spline | Basis spline |
| $c$ | Blade chord |
| $c_d$ | 2D Drag coefficient |
| $c_l$ | 2D Lift coefficient |
| $\mathcal{C}_{\mathcal{L}}$ | Operator used to calculate $c_l$ |
| CDF | Cumulative distribution function |
| CFD | Computational fluid dynamics |
| D | Propeller diameter |
| $F$ | Cost function |
| $G$ | Goldstein circulation function |
| $G_i$ | Constraint |
| $g_i$ | Constraint coefficients |
| gPC | Generalized polynomial chaos |
| HAPS | High-Altitude Pseudo-Satellites |
| $i_0$ | Zero load current |
| $K_P$ | Power coefficient, $\frac{P}{0.5\rho\pi R^2 V^3}$ |
| $K_Q$ | Torque coefficient, $\frac{Q}{0.5\rho\pi R^2 V^3}$ |
| $K_T$ | Thrust coefficient, $\frac{T}{0.5\rho\pi R^2 V^2}$ |
| $K_v$ | Speed constant |
| $M$ | Total number of basis functions |
| Ma | Mach number |
| MC | Monte Carlo method |
| $n$ | Propeller revolutions per second |
| $n_{\text{crit}}$ | Critical amplification factor used in XFOIL |
| NCAR | National Center for Atmospheric Research |
| NCEP | National Centers for Environmental Prediction |
| $P$ | Power/ Approximation order of the polynomial |
| $P_e$ | Electric power |
| $P_s$ | Mechanical power |
| PDF | Probability density function |

| | |
|---|---|
| $Q$ | Torque |
| $r$ | Geometry scale |
| $R$ | Propeller radius |
| $\mathcal{R}$ | Motor resistance |
| Re | Reynolds number |
| RMS | Root mean square |
| rpm | Revolutions per minute |
| $\mathbf{X}$ | Multivariate random variable |
| XFOIL | Interactive program for the analysis of subsonic airfoil |
| $S$ | Multivariate random variable |
| $S_i$ | Univariate random variable |
| SL | Sea level |
| $T$ | Thrust |
| $Tu_\infty$ | Turbulence levels (%) |
| $U_0$ | Resultant velocity at a blade element |
| $\overline{u}_{\theta_0}$ | Induced velocity in the radial direction |
| $\overline{u}_{z_0}$ | Induced velocity in the axial direction |
| $\mathfrak{v}$ | Motor terminal voltage |
| $V$ | Fluid velocity |
| $\mathbf{Y}$ | Multivariate stochastic function |
| $\hat{\mathbf{Y}}$ | Multivariate stochastic function approximation |
| $\hat{\mathbf{Y}}_i$ | gPC expansion coefficients |
| $\overline{w}$ | Backward velocity of the vortex sheet |
| $\alpha$ | Angle of attack |
| $\beta$ | Blade angle from plane of rotation |
| $\Gamma$ | Circulation, $\oint v \mathrm{d}\mathbf{x}$ |
| $\eta$ | Net propulsion efficiency |
| $\eta_a$ | Aerodynamic efficiency, $\frac{K_T}{K_P}$ |
| $\eta_m$ | Motor performance |
| $\delta_{ij}$ | Kronecker delta function |





Please cite this article in press as: García-Gutiérrez, A., Gonzalo, J., López, D., Delgado, A (2020). Stochastic design of high altitude propellers. *Aerospace Science and Technology*, 107, 106283, https://www.sciencedirect.com/science/article/pii/S1270963820309652

| | |
|---|---|
| $\phi$ | One dimensional polynomial basis function |
| $\phi_0$ | Pitch angle |
| $\Phi_i$ | Multivariate orthogonal polynomial basis function |
| $\lambda$ | Advance ratio, $\frac{V}{\Omega R}$ |
| $\lambda_2$ | Advance ratio of the trailing helicoidal vortex sheet |
| $\mu$ | Kinematic viscosity/mean |
| $\rho$ | Air density |
| $\varrho$ | Joint probability density function |
| $\rho_i$ | Probability density function of the $i$th of $S_i$ |
| $\nu$ | Kinematic viscosity |
| $\sigma$ | Standard deviation |
| $\sigma_b$ | Blade solidity factor, $\frac{Bc}{2\pi R}$ |
| $\Omega$ | Propeller Angular Velocity |

## 1. Introduction

Propellers were one of the first aeronautical propulsion devices used. However, they are commonly used in unmanned aerial vehicles, general aviation and stratospheric platforms —also called HAPS. Usually, the propeller design has an enormous influence on the efficiency of the whole propulsion system. Unfortunately, their aerodynamic design is largely affected by uncertainties. The sources of these uncertainties are mainly related to the highly stochastic nature of the wind [1] and to the limited fidelity of the aerodynamic models that are used. Uncertainties also appear in material properties, wearing of the blades over time as well as many other aspects [2] of the motor and its operating environments. All those uncertain factors affect the aerodynamic performance and the propulsion system's lifetime. The inadequate treatment of uncertainty has a significant effect in the design requirements under off-design conditions, which can be of utmost importance for High-Altitude Pseudo-satellites (HAPS).

However, much of the research up to now does not consider uncertainty. For





Please cite this article in press as: García-Gutiérrez, A., Gonzalo, J., López, D., Delgado, A (2020). Stochastic design of high altitude propellers. *Aerospace Science and Technology*, 107, 106283, https://www.sciencedirect.com/science/article/pii/S1270963820309652

example, in most of the design algorithms [3], the ideal propeller is designed for a particular wind speed. Initially, this makes sense as, for example, a common mission requirement for an stratospheric airship is to perform station keeping in the presence of a stationary wind field of constant intensity. However, the whole mission performance relies on a good selection of the speed at which the propeller is supposed to operate most of the time. Under real conditions, that wind speed varies with time [4], following a statistical distribution [5]. How this wind distribution affects the propeller design and its performance has not been treated before.

Apart from the wind, there are other sources of uncertainty such as the low Reynolds phenomena [6]. That phenomena characterizes the stratospheric propellers and causes a high variability in the aerodynamic coefficient of the blade sections [7]. The high variability makes impossible to assure the aerodynamic performance of the propeller. To date, the problem has received scant attention in the research literature.

In order to solve equations involving randomness, the traditional approach is to use the Monte Carlo (MC) method [8], which is based on generating a large number of samples from random realizations of the input data. Although it is a very robust method, the main problem is that the convergence rate of the MC method is very slow [9]. On the other hand, the generalized polynomial chaos method (gPC) [10] evaluates solutions of the stochastic system at carefully chosen points within the random space to compute accurate statistics with significantly fewer system evaluations than MC methods.

In this work, we will employ the gPC approach to perform efficient optimization in the presence of uncertainty. One of the main advantages of the method described is that it can be implemented by re-using design software from other pre-existing deterministic methods [11], which can be interwoven with the evaluation of the design cost function at the evaluation points. Moreover, it can also be adapted to include a large number of uncertainties [12] and to find global solutions [13].

The article is organized as follows. In Section 2, we introduce the generalized polynomial chaos expansion and we explain how it can be used for design purposes in Section 3. In order to apply it to the design of a stratospheric propeller, we present one of the deterministic methods that has been traditionally used and is required by the stochastic method in 4. Next, the main sources of uncertainty are studied in Section 5, which are the wind speed fluctuations and the variability in the aerodynamic coefficients. Finally, in Section 6, the design method is applied to an airship that requires a thrust of 100 N and the conclusions are summarized in Section 7.

## 2. Non intrusive polynomial chaos

The gPC [14] method approximates a stochastic solution $\mathbf{Y} = \mathbf{Y}(\mathbf{S})$ of the design problem by a finite linear combination of the orthogonal polynomials $\phi_i$ of $N$- independent random variable $\mathbf{S} = (S_1, \ldots, S_N) \in \mathbb{R}^N$. The $P$th order approximation of the stochastic design solution $\mathbf{Y}(\mathbf{S})$ can be written as:

$$\mathbf{Y}(\mathbf{S}) \approx \hat{\mathbf{Y}}(\mathbf{S}) := \sum_{i=0}^{M} \hat{\mathbf{Y}}_i \Phi_i(\mathbf{S}), \tag{1}$$

where $\hat{\mathbf{Y}}_i$ are the gPC expansion coefficients, and $\Phi_i(\mathbf{S})$ are the multivariate orthogonal polynomial basis functions which can be written in terms of one-dimensional polynomial basis functions $\phi_i^{(l_i)}(S_i)$ of each random variable $S_i$ according to the following relation:

$$\Phi_i(\mathbf{S}) = \prod_{i=1}^{N} \phi_i^{(l_i)}(S_i), \tag{2}$$

where $\sum l_i \leq P$ and the coefficient $M$ is the total number of basis functions and can be calculated as $M = \binom{N+P}{M}$.

The polynomial base is orthogonal under the following vector product:

$$\langle \phi_i(S_i), \phi_j(S_i) \rangle = \delta_{ij} \langle \phi_i(S_i)^2 \rangle, \tag{3}$$

where $\langle \cdot, \cdot \rangle$ is defined as the expectation operator:

$$\langle f(S_i), g(S_i) \rangle = \int f(S_i) g(S_i) \rho_i(S_i) \mathrm{d}S_i, \tag{4}$$

being $\rho_i(S_i)$ the probability density function (PDF) corresponding to the $i$th random variable $S_i$ and $\delta_{ij}$ the Kronecker delta function.

In order to compute each of the coefficients $\hat{\mathbf{Y}}_i$, we can apply the expectation operator to the orthogonal polynomial $\Phi_i(\mathbf{S})$ which yields to the following equation:

$$\hat{\mathbf{Y}}_i = \frac{1}{\langle \phi_i(\mathbf{S})^2 \rangle} \int f(\mathbf{S}) \Phi_i(\mathbf{S}) \varrho(\mathbf{S}) \mathrm{d}\mathbf{S}. \tag{5}$$

where $\varrho$ is the joint probability density function $\varrho(\mathbf{S}) = \prod \rho_i(S_i)$. Efficient algorithm to calculate these coefficients are shown in the studies of Golub [15] and Gautschi [16] but they are already implemented in scientific toolboxes such as Chaospy [17].

The integral of Eq. (5) can be approximated by quadrature, so the following expression is obtained:

$$\hat{\mathbf{Y}}_i = \sum_{k_1=1}^{m_1} \cdots \sum_{k_q=1}^{m_q} \mathbf{Y}(s_{k_1} \cdots s_{k_q}) \frac{\Phi_i(s_{k_1} \cdots s_{k_q})}{\langle \Phi_i(s_{k_1} \cdots s_{k_q})^2 \rangle} \prod_{j=1}^{q} \omega_j, \tag{6}$$

being $s_{k_j}$ with $j = 1 \cdots q$ the quadrature points of the $j$th-component of the random vector $\mathbf{S}$, $m_i$ denotes the integration points number of each random variable and $\omega_j$ is the quadrature $j$th-dimension weight of the point $s_{k_j}$. There are different kinds of quadrature than can be used such as Gaussian [18], Fejer [19] or Clenshaw-Curtis [20].

Once the coefficients have been computed, the expected value $\mu$ and the variance $\sigma$ of $\mathbf{Y}(\mathbf{S})$ can be estimated using the following equations:

$$\mu(\mathbf{Y}(\mathbf{S})) \approx \hat{\mathbf{Y}}_0, \tag{7}$$

$$\sigma(\mathbf{Y}(\mathbf{S})) \approx \sqrt{\sum_{i=1}^{p} \langle \phi_i^2 \rangle \hat{\mathbf{Y}}_i}. \tag{8}$$

This method is a non intrusive algorithm i.e., it only requires to simulate a deterministic model at some sampling points [21], so traditional design codes can be re-utilized. The evolution of uncertainty in a dynamic system can also be determined by means of intrusive methods [22]. However, they require modifications of the original equations and they need to derive new stochastic models which are developed from the first principles of a system [23].

## 3. Design methodology

The probabilistic information obtained from the approximated stochastic solution can be used as part of the cost function as well as to evaluate constraints in the design. Thus, both the design point performance and the probabilistic information —such as its mean performance during operation or confidence intervals— are relevant for the optimization problem. Using the quadrature points in the non intrusive PC expansion $S_k = (s_{k_1} \cdots s_{k_q})$ along with Eqs. (7) and (8), the stochastic design problem can be converted into an equivalent deterministic one. In the most general case:

$$\begin{aligned} \min\ F(\mathbf{X}, \mathbf{Y}_1, \cdots, \mathbf{Y}_n, \mathbf{S}), \\ \mathbf{Y}_1 = \mathbf{F}(\mathbf{X}, S_1), \\ \vdots \\ \mathbf{Y}_n = \mathbf{F}(\mathbf{X}, S_n), \\ \mathbf{G}_1(\mathbf{X}, \mathbf{Y}_1, \cdots, \mathbf{Y}_n, \mathbf{S}) > g_1, \\ \vdots \\ \mathbf{G}_m(\mathbf{X}, \mathbf{Y}_1, \cdots, \mathbf{Y}_n, \mathbf{S}) > g_m, \end{aligned} \tag{9}$$

where $F(\mathbf{X}, \mathbf{Y}_1, \cdots, \mathbf{Y}_n, \mathbf{S})$ is a generic function that represents the cost function, $\mathbf{X}$ is a vector of the design variables, and the different $G_i(\mathbf{X}, \mathbf{Y}_1, \cdots, \mathbf{Y}_n, \mathbf{S})$ represent the constraints with $g_i$ being known coefficients.

The main advantage of this methodology is that it can be easily implemented using traditional modeling methods (represented here by the function $\mathbf{F}$): it is not necessary to change their inner implementation just to use them in different design points. The general procedure can be described as follows:

1. Select one of the deterministic modeling methods $F(\mathbf{X})$ that are available in literature.
2. Determine the random variables $\mathbf{S}_i$ that take part in the design e.g. wind, geometrical uncertainties, etc.
3. For each of these variables, determine its probabilistic distribution functions $\rho_e$.

4. Using Eqs. (3) and (4), calculate the proper orthogonal basis for each of the variables, which depends on the probabilistic distribution functions of Step 3.
5. Compute the quadrature points and weights of Eq. (6).
6. Solve the deterministic optimization problem of Eq. (9).

## 4. Deterministic analysis method

The propulsion system of a High Altitude Pseudo-Satellites (HAPS) [24] traditionally consists of propellers which are driven by electric motors. Below, a model is presented for each of the components. Both models can be used to compute the overall system performance once they are coupled. In the present study, the design variables are the chord and pitch angle distributions along the blade. Being $\eta_a$ the aerodynamic performance of the propeller and $\eta_m$ the motor performance, the net propulsive efficiency is given by $\eta_p = \eta_a \eta_m$. Typical values of $\eta_a$ for stratospheric platform oscillates between 0.4-0.6 [25].

### *4.1. Propeller analysis*

Traditionally, the different approaches[25] used to design a propeller rely on the inverse design method, which defines the required blade geometry for a predefined operational point, trying to optimize the total efficiency of the propeller $\eta_a$. The analysis has nearly always been based on the lifting line theory [26, 27]. Blade elements are considered to act as two-dimensional airfoils in which the lift and drag are the same, as would be found in a uniform two dimensional flow with the same velocity and attack angle. For the present analysis, this approach is also followed.

Once the airfoil shape is selected, the geometry of the propeller is mainly characterized by its chord and pitch angle distributions. B-splines[28] have been traditionally used to make the blade shape smooth and continuous along the spanwise direction. The diameter of the propeller and the number of blades are taken here as an input parameter for the design algorithm. It is well known that increasing the propeller diameter increases the efficiency [29]. That performance augmentation is thanks to the high aspect ratio, which helps to counteract the efficiency losses caused by the blades interference. However, the weight and the structural strength [28] are also important trade-off parameters that limit the blade dimensions.

We will follow the methodology described in Wald [30]. The reader is encouraged to follow the original paper for more detail, however, the main steps of the algorithm are detailed here. For a given advance ratio $\lambda$, number of blades $B$, radius $R$, blade angle distribution $\beta(x)$, chord $c(x)$ and airfoils along the blade an iterative procedure is developed to determined the characteristic of the vortex sheet generated by the propeller. Once that has been carried out, the aerodynamic coefficients of the propeller can be found.

For each section of the blade, the algorithm can be described as follows:

1. Suppose a initial value of the $\overline{w}(x)$ which represents the backward velocity —divided by the propeller's forward speed— of the vortex sheet with respect to the air.
2. The advance ratio of the trailing helicoidal vortex sheet, far from the propeller, can be calculated as $\lambda_2 = \lambda(1+\overline{w})$ being $\lambda$ the advance ratio of the propeller.
3. The circulation originated by that vortex sheet gives us the lift generated in each section:
$$c_l = 2\lambda\overline{w}(1+\overline{w})\frac{G(x,\lambda_2)}{\left(\frac{U_0}{V}\right)\sigma_b} \tag{10}$$
in which $G(x,\lambda_2)$ represents the Goldstein function, $\sigma$ is the blade solidity and $\frac{U_0}{V}$ is the ratio between the local wind speed and the forward speed. There are several methods to calculate the Goldstein [31] circulation as in Ribner and Foster [29], but it was also tabulated by Wald [30]. This function gives the optimal circulation along the blade which produces minimum induced losses.
4. Then, the induced velocities in the radial and axial direction —each one

also divided by the forward speed— can be computed as:

$$\overline{u}_{\theta_0} = \frac{1}{2}\overline{w} + (1+\overline{w})\frac{\lambda}{x_0(1+\left[\frac{\lambda_2}{x_1}\right]^2)}, \tag{11}$$

$$\overline{u}_{z_0} = \frac{1}{2}\frac{\overline{w}}{1+\left(\frac{\lambda_2}{x_1}\right)^2}. \tag{12}$$

being $x_0$ the radial position of the propeller's root and $x_1$ the radial position of the blade's section. Both magnitudes are non-dimensionalized by the propeller's radius.

5. So the total velocity of each section is:

$$\left(\frac{U_0}{V}\right)^2 = (1+\overline{u}_{z_0})^2 + (\frac{x_0}{\lambda} - \overline{u}_{\theta_0})^2, \tag{13}$$

6. The following equation let us to calculate the pitch angle of the relative wind:

$$\tan\phi_0 = \frac{V+\overline{u}_{z_0}}{\frac{x_0}{\lambda} - \overline{u}_{\theta_0}}. \tag{14}$$

7. The attack angle of each airfoil is given by:

$$\alpha = \beta - \alpha_{L_0} \tag{15}$$

8. Finally, the $c_l$ of each section can be calculated. In general, it will be a function of the freestream Reynolds number $\mathrm{Re} = \frac{\rho c U_0}{\nu}$, the Mach number $\mathrm{Ma} = \frac{U_0}{a}$ and the turbulence levels (represented here by the parameter $n_{\mathrm{crit}}$):

$$c_l = \mathcal{C}_{\mathcal{L}}(n_{\mathrm{crit}}, \mathrm{Ma}, \mathrm{Re}, \alpha) \tag{16}$$

We will see in the next subsection how the aerodynamic coefficients have been calculated in the present study, although different alternatives are available e.g. potential codes, CFD simulations, experimental data.

9. Check the difference between the $c_l$ calculated in Eq. (10) with the value of Eq. (16) and change the value of $\overline{w}$ until that difference is under a determined threshold.





Please cite this article in press as: García-Gutiérrez, A., Gonzalo, J., López, D., Delgado, A (2020). Stochastic design of high altitude propellers. *Aerospace Science and Technology*, 107, 106283, https://www.sciencedirect.com/science/article/pii/S1270963820309652

Once the correct value of $\overline{w}$ has been found, the thrust and torque coefficients can be calculated as follows:

$$K_T = 2\int_0^1 \left(c_l \cos\left(\phi_0\right) - c_d \sin\left(\phi_0\right)\right)\left(\frac{U_0}{V}\right)^2 \sigma \mathrm{d}x, \tag{17}$$

$$K_Q = 2\int_0^1 \left(c_l \sin\left(\phi_0\right) + c_d \cos\left(\phi_0\right)\right)\left(\frac{U_0}{V}\right)^2 \sigma x \mathrm{d}x, \tag{18}$$

$$\tag{19}$$

so the aerodynamic efficiency of the propellers is given by:

$$\eta_a = \frac{\lambda K_T}{K_Q}. \tag{20}$$

### *4.2. Electric motor model*

Apart from the propeller, it is also relevant to estimate the performance of the electric motor. A DC electric motor can be modeled using a first order circuit with the following equations [32, 33]:

$$Q_m(i) = \frac{(i - i_0)}{K_v}, \tag{21}$$

$$\Omega(i, \mathfrak{v}) = (\mathfrak{v} - i\mathcal{R})K_v, \tag{22}$$

$$P_s(i, \mathfrak{v}) = Q_m\Omega = (i - i_0)(\mathfrak{v} - i\mathcal{R}), \tag{23}$$

$$P_e(i, \mathfrak{v}) = \mathfrak{v}i, \tag{24}$$

$$\eta_m(i, \mathfrak{v}) = \frac{P_s}{P_e} = \frac{1 - i_0/i}{1 - i\mathcal{R}/\mathfrak{v}}, \tag{25}$$

in which $\mathfrak{v}$ is the terminal voltage, $i_0$ is the zero-torque current, $i$ is the current, $Q_m$ is the generated torque, $K_v$ is the speed constant, $\mathcal{R}$ is the equivalent resistance, $\Omega$ is the angular speed of the rotor, and $P_s$, $P_e$ denote, respectively, the effective and consumed power.

We are only interested in the motor efficiency as function of the torque and rotation rate of the propeller. The Eqs (21)-(25) can be rearranged to obtain:

$$v(\Omega, Q) = (K_v Q + i_0)\mathcal{R} + \frac{\Omega}{K_v} \tag{26}$$

$$\eta_m(\Omega, \mathfrak{v}) = \left[1 - \frac{i_0\mathcal{R}}{\mathfrak{v} - \frac{\Omega}{K_v}}\right]\frac{\Omega}{\mathfrak{v}K_v} \tag{27}$$





Please cite this article in press as: García-Gutiérrez, A., Gonzalo, J., López, D., Delgado, A (2020). Stochastic design of high altitude propellers. *Aerospace Science and Technology*, 107, 106283, https://www.sciencedirect.com/science/article/pii/S1270963820309652

## 5. Uncertainty in design variables

As we mentioned in the introduction, two sources of uncertainty will be tackled: the wind intensity and the variability of aerodynamic coefficients at low Reynolds number.

### 5.1. Wind

Following previous studies [34], we have characterized the wind distribution at the stratosphere using the available meteorological data from the NCEP/NCAR reanalysis project [35]. These data consist of global analyses of atmospheric fields from 1948/01/01 up to the present day (2020/04/01), 4 times per day, with spatial resolution of 2.5° in both latitude and longitude. The available pressure levels are in the range between $10^3$ and 10 mbar, so the typical operational level of stratospheric platforms —around 20 km or 55 mb— falls within the range.

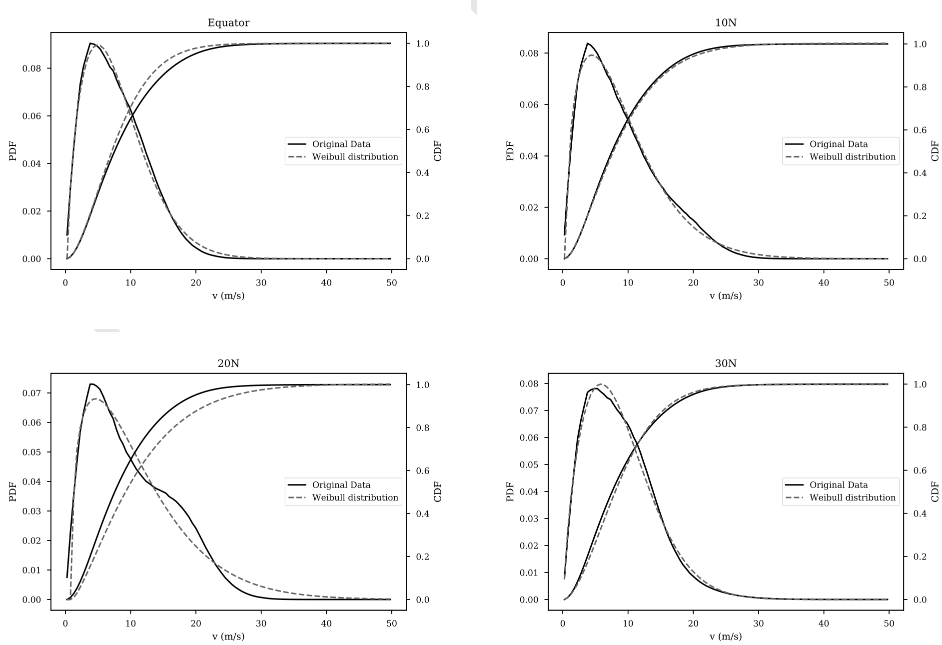


Figure 1: Probability and cumulative density function of the wind speed for latitudes at 30°, 20°, 10° and the Equator.



Please cite this article in press as: García-Gutiérrez, A., Gonzalo, J., López, D., Delgado, A (2020). Stochastic design of high altitude propellers. *Aerospace Science and Technology*, 107, 106283, https://www.sciencedirect.com/science/article/pii/S1270963820309652

With all these data, the wind intensities PDFs have been calculated for different altitudes and are plotted in Figure 1.

### 5.2. Low Reynolds phenomena

As we have seen in Section 4, it is required to calculate the aerodynamic coefficients of the airfoils for different Reynolds/Mach numbers. The use of two dimensional codes, which combine panel methods and boundary layer models, such as XFOIL, is extended in the literature [26, 36] for preliminary design. XFOIL is a vortex panel method code which uses the $e^N$ theory to capture the boundary layer transitions; the theory states that the disturbance in the linearized boundary layer equations grows $e^{n_{\text{crit}}}$ times before passing to turbulence i.e. $n_{\text{crit}}$ is the log of the amplification factor of the most amplified wave which initiates the transition.

In reality, a high variability can be noticed in the aerodynamic coefficients of the airfoils mainly due to the low Reynolds number [37] at which the stratospheric propellers operate [38, 39, 40]. Following the work of Caboni, Minisci and Riccardi [41], this uncertainty is modeled by means of the parameter $n_{\text{crit}}$ [42] in order to represent the background turbulence levels. An empirical correlation between the turbulence levels $Tu_\infty$ (in %) and the value of $n_{\text{crit}}$ was found by Mack [43]:

$$n_{\text{crit}} = -8.43 - 2.4 \log (Tu_\infty), \tag{28}$$

The previous equation produced negative $n_{\text{crit}}$ values when the turbulence levels are larger than 2.98%. The modified definition proposed by Shaw[44] is:

$$Tu'_\infty = 2.7 \tanh \left( \frac{Tu_\infty}{2.7} \right), \tag{29}$$

$$n_{\text{crit}} = -8.43 - 2.4 \log \left( \frac{Tu'_\infty}{100} \right), \tag{30}$$

which is equivalent to the original relation for low turbulence levels and goes asymptotic to zero for large turbulence levels.

In the present study it is considered that the turbulence levels follow a Gaussian distribution as a consequence of the central-limit theorem [45]. A value

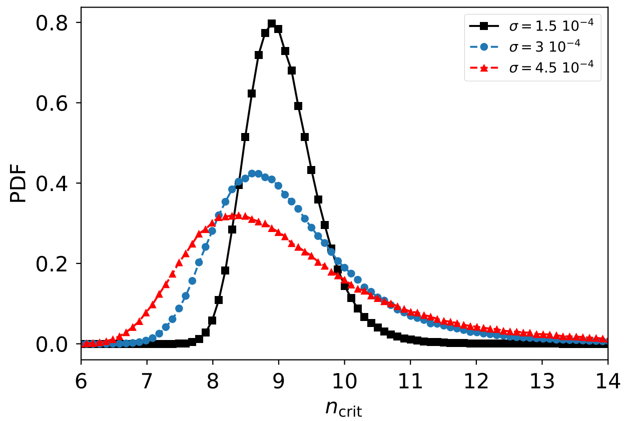


Figure 2: PDF of $n_{\mathrm{crit}}$ for different values of turbulence levels variance. In all the cases, the turbulence levels are considered to follow a Gaussian distribution with mean $\mu = 0.7\%$.

of $n_{\mathrm{crit}} = 9.0$ is typically used [46] for the preliminary design as in Morgado [26] and Gamboa [36]. This value is obtained when $Tu_\infty = 0.07\%$ so it can be taken as the mean value.

However, it is necessary to estimate the standard deviation $\sigma$ of the Gaussian distribution. Figure 2 shows how the distribution varies for different $\sigma$. In order to select the best value of $\sigma$ it is necessary to study the experimental data available. Although that data is scarce, we will focus on the NACA4412, which is one of the most common airfoils for low Reynolds operation. Using the available data from the tests in Simmons [47], Eastman [48], Koca [49], and the University of León [34], the Figure 3 compares those results with the range in which the aerodynamic efficiency of the airfoil oscillates for standard deviations between $\sigma = 3\,10^{-4}$ (gray) and $\sigma = 1.5\,10^{-4}$ (red).

For $\mathrm{Re} = 7.5\,10^4$, there is a small difference between choosing $\sigma = 3\,10^{-4}$ or $\sigma = 1.5\,10^{-4}$. Both values achieve to simulate the uncertainty generated by the low Reynolds phenomena: they generate confidence intervals which contains almost all the experimental results available in literature. However, for $\mathrm{Re} = 4.5\,10^4$, the experiment results obtained by Eastman [48] differ notably from the others. That difference cannot be captured by any value of $\sigma$ so it





Please cite this article in press as: García-Gutiérrez, A., Gonzalo, J., López, D., Delgado, A (2020). Stochastic design of high altitude propellers. *Aerospace Science and Technology*, 107, 106283, https://www.sciencedirect.com/science/article/pii/S1270963820309652

might be originated to another kind of uncertainty. There also some values of Simmons [47] and Koca [49] which are not captured and may be related to numerical/model errors when the Reynolds number is too low.

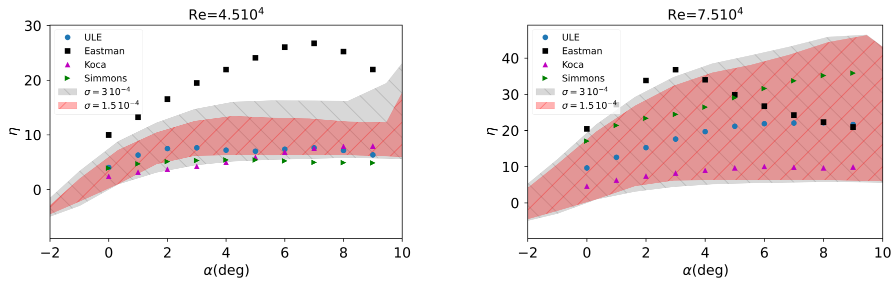


Figure 3: Range of the $\eta$ when the turbulence levels follow the probabilistic distribution of Figure 2 for $\sigma = 3\,10^{-4}$ and $\sigma = 1.5\,10^{-4}$. Experimental data from the University of León [34] from Simmons [47], Eastman [48], and Koca [49].

The parameter $n_{\mathrm{crit}}$ has a relevant effect in the aerodynamic coefficients. Figure 4 shows how the maximum efficiency varies for different values of $\alpha$ and $n_{\mathrm{crit}}$. A relevant loss in the aerodynamic efficiency can be observed for low Reynolds numbers, specially when the values of $n_{\mathrm{crit}}$ are high. The reason for this is related to the formation of re-circulation bubbles [50].





Please cite this article in press as: García-Gutiérrez, A., Gonzalo, J., López, D., Delgado, A (2020). Stochastic design of high altitude propellers. *Aerospace Science and Technology*, 107, 106283, https://www.sciencedirect.com/science/article/pii/S1270963820309652

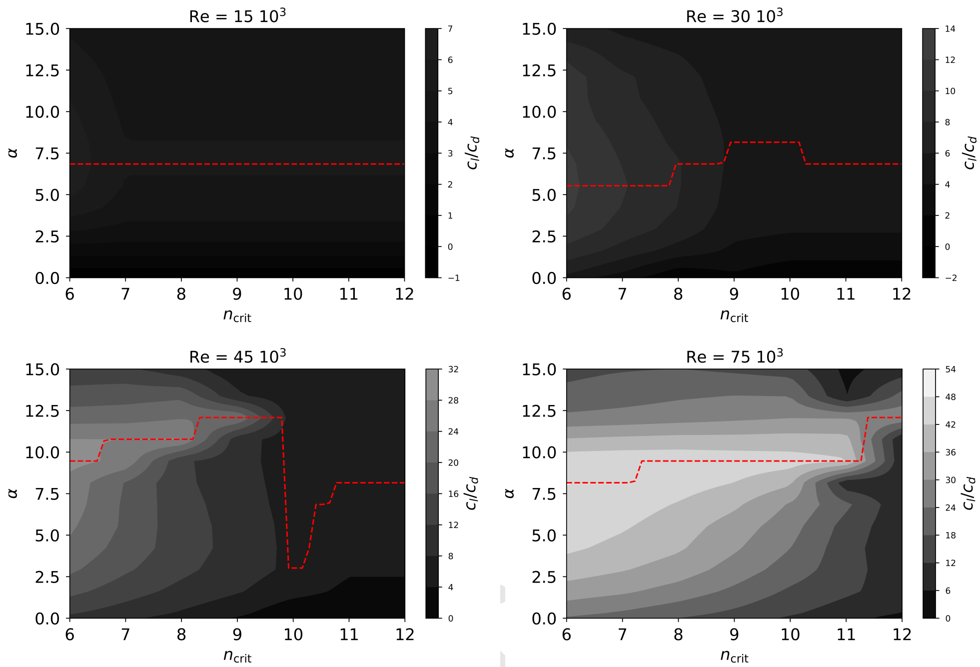


Figure 4: Aerodynamic efficiency as function of the $\alpha$ and $n_{\text{crit}}$. From left to right, top to bottom: Reynolds number of $1.5\,10^4$, $3.0\,10^4$, $4.5\,10^4$ and $7.5\,10^4$. The dashed line marks the maximum aerodynamic efficiency.

## 6. Case of Study

Next, we apply the optimized algorithm to a HAPS airship operating in the stratosphere —20 km— at a latitude of 30° N. We can see from Figure 1 that the mean wind speed value is around 9 m/s. With a 400 kg payload and a total length of 90 m, using two propellers, the thrust required by each of them is approximately 100 N [24].

Regarding the airfoil, we will consider that the propeller sections are given by the NACA4412 airfoil so the study carried out in Section 5 can be used. For our case, the design variables are the control points of the B-splines that are used to represent the chord and pitch angle distribution along the blade and the propeller radius is fixed to 3.5 m. The number of blades is also fixed to four. Two main sources of uncertainty are take into account: the wind intensities, following the PDF of Figure 1 for 30°N latitude; and the aerodynamic coefficients, in which we suppose that the turbulent levels follows a Gaussian distribution of mean 0.07% and $\sigma = 0.035\%$.

The electric motor used for this study is similar to that used by MacNeill [51] and Peponakis [52] but adapted to higher torques, with the following values speed constant $K_V = 1\,\mathrm{RPM/V}$, internal resistance $\mathcal{R} = 0.7\,\Omega$ and zero-load current $i_0 = 0.6\,\mathrm{A}$. The motor performance is also similar to the one studied by Bogus [53]. These parameters are constant during the optimization.

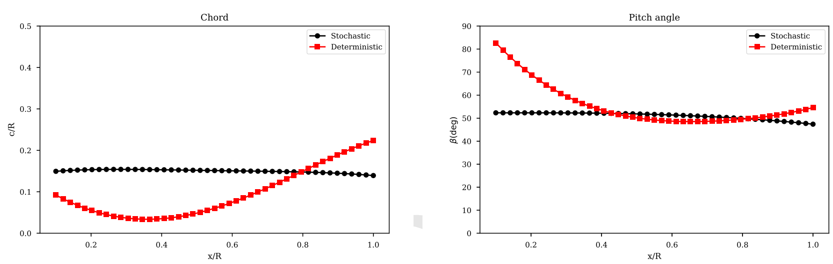


Figure 5: Changes in the chord and pitch angle optimization when the optimization is done with the new method proposed. These designs generate 100 N at a wind speed of 9 m/s.

The cost function is defined as the mean of the propulsion system efficiency $\langle \eta_p \rangle$. Apart from that, there is an additional constraint: for each value of wind speed and turbulence level, the propeller must operate at the same $C_T$. With that constraint, we simulated the situation in which a stratospheric airship tries to remain at a fixed position independently of the wind intensity. More complex control laws [54] can be study in future works.

The algorithm used to solve the optimization problem was the trust-region constrained method [46]. The Gauss-Radau quadrature [55] was selected for the polynomial expansion. The results using the optimization algorithm are compared against the case in which the wind speed is supposed to remain constant at $9s\,\mathrm{m}/$ and a value of $n_{\mathrm{crit}} = 9.0$ in Figure 5. The pitch angle and chord distributions have a nearly constant value for all the propeller sections. This



Please cite this article in press as: García-Gutiérrez, A., Gonzalo, J., López, D., Delgado, A (2020). Stochastic design of high altitude propellers. *Aerospace Science and Technology*, 107, 106283, https://www.sciencedirect.com/science/article/pii/S1270963820309652

finding was unexpected and suggests that for the low Reynolds number regime, the parasitic drag is more relevant for the optimization than the induced one. This observation may support the hypothesis that, when the propeller is not operating at a fixed point, it does not make sense trying to reduce only the induced drag. Instead, it is more useful to find the angle in which the maximum aerodynamic efficiency is achieved. An explanation for these pitch angle and chord distribution to be constant has not been determined yet, but these conclusions can help to find more robust designs [56].

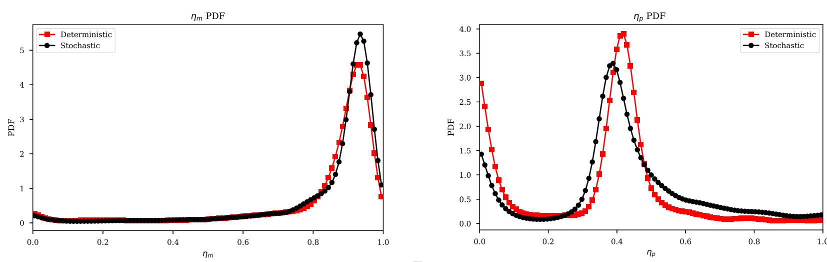


Figure 6: Comparison between the deterministic and stochastic optimization results for the case of Figure 5. Left: electric motor efficiency. Right: net propulsion efficiency.

A Montecarlo test has been performed to evaluate how well each of the two designs works. Under the assumption that the wind speed and the turbulence levels follow the mentioned distributions, 5000 samples have been generated and computed for each design, obtaining the performance of both propulsion system components. The propulsion and electric motor efficiencies are shown in Figure 6. While the motor's performance remains similar in both cases, the mean of the propulsion system efficiency improves from 0.21 to 0.26, which is an augmentation of 5%. These values can be computed integrating the PDF, following the Equation:

$$\mu(\eta_i) = \int_0^1 \eta_i \varrho_{\eta_i} \mathrm{d}\eta_i \tag{31}$$

where $\eta_i$ is the efficiency ($\eta_p$, $\eta_a$ or $\eta_m$) and $\varrho_{\eta_i}$ is its PDF. Most of this increment is achieved thanks to the extension of the propulsion system operational regime, i.e. the design robustness. There are combinations of wind speed and $n_{\text{crit}}$ values in which the propulsion system cannot not work (overload, insufficient speed, etc.). However, the frequency of this events is decreased by a 10% when the optimization is done taking into account the uncertainties.

One unanticipated finding was that this optimal design is constant for a certain range of required thrust. For example, we can repeat the study for a slightly different case. The same airship and wind conditions are used but using only one propeller instead of two. The results using the optimization algorithm are compared against the case in which the wind speed is supposed to remain constant at $9\,\mathrm{m/s}$ and a value of $n_{\mathrm{crit}} = 9.0$ in Figure 7. The design obtained in the deterministic case is clearly different: it needs to generate more thrust so the blade's solidity must be higher. Surprisingly, the stochastic design is almost equal that in the previous case.

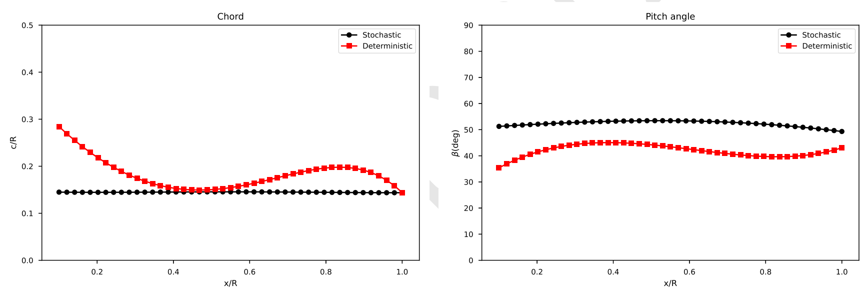


Figure 7: Changes in the chord and pitch angle optimization when the optimization is done using the stochastic method. These designs generate 200 N at a wind speed of 9 m/s.

We also repeated the Montecarlo test in similar conditions than the previous one. The propulsion and electric motor efficiencies are shown in Figure 8. In this case, the stochastic design presents a net loss in the motor efficiency, although the increment in the aerodynamic efficiency compensates for the previous loss. The mean propulsion system efficiency improves from 0.2 to 0.25, which is an augmentation of 5%. Most of this increment is also achieved thanks to an improvement in the design robustness.



Please cite this article in press as: García-Gutiérrez, A., Gonzalo, J., López, D., Delgado, A (2020). Stochastic design of high altitude propellers. *Aerospace Science and Technology*, 107, 106283, https://www.sciencedirect.com/science/article/pii/S1270963820309652

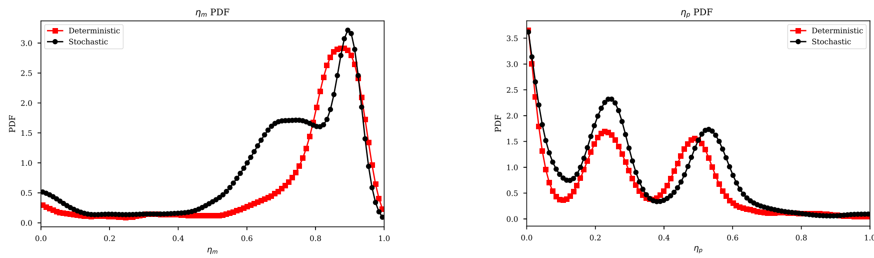


Figure 8: Comparison between the deterministic and stochastic optimization for the case of Figure 7. Left: electric motor efficiency of the propeller. Right: net propulsion efficiency.

## 7. Conclusions

This study has presented a methodology to optimize stratospheric propellers in an uncertain design scenario. The generalized polynomial chaos theory [57] has been used as a tool that transforms the stochastic optimization problem into an deterministic one. Two main sources of uncertainty have been considered. Firstly, the wind intensity at the stratosphere has been characterized for different latitudes. Secondly, based on experimental data, we have shown how some of the uncertainty in the aerodynamic coefficients of the airfoil at low Reynolds number can be modeled using the $n_{crit}$ value of the $e^N$ transition theory. Uncertainty has been related mainly to the wind intensity and the turbulence levels, which modify the aerodynamic coefficient of each section.

As a particular application, the shape of a propeller for large stratospheric airships has been optimized. Operating at 20 km and 30°N, and with a required thrust of 100 N, two optimal designs have been calculated: the first one, without taking into account uncertainties, and the second one including how the wind and aerodynamic coefficients vary. The blade chord and pitch distributions have been discretized using B-splines and the optimal problem was solved using the trust-region algorithm. When the uncertainties are taken into account, the chord and pitch angle distributions remains almost constant for the different blade sections.

In order to check the utility of the previous design method, a Montecarlo





Please cite this article in press as: García-Gutiérrez, A., Gonzalo, J., López, D., Delgado, A (2020). Stochastic design of high altitude propellers. *Aerospace Science and Technology*, 107, 106283, https://www.sciencedirect.com/science/article/pii/S1270963820309652

experiment has been done generating a large number of samples of wind intensity and turbulence levels. For each sample, the performances of the stochastic and deterministic design have been computed. The results show that the stochastic design improves the mean net propulsion efficiency by a 5% for this particular case of study. This gain is of utmost importance for HAPS operations [34, 58] and is mostly related to an improvement in the design robustness.

Future work will investigate the propeller design under more complex operation scenarios and control laws, and asses the computational cost.

## Declaration of Competing Interest

The authors declare that there is no conflict of interests regarding the publication of this article.

## Acknowledgements

The authors acknowledge the valuable suggestions of the anonymous referees that helped to enhance the manuscript.

## References

[1] Y. Matsuno, T. Tsuchiya, J. Wei, I. Hwang, N. Matayoshi, Stochastic optimal control for aircraft conflict resolution under wind uncertainty, Aerospace Science and Technology 43 (2015) 77 – 88. doi:https://doi.org/10.1016/j.ast.2015.02.018. URL http://www.sciencedirect.com/science/article/pii/S1270963815000759

[2] Z. Xia, J. Luo, F. Liu, Performance impact of flow and geometric variations for a turbine blade using an adaptive nipc method, Aerospace Science and Technology 90 (2019) 127 – 139. doi:https://doi.org/10.1016/j.ast.2019.04.025.

URL http://www.sciencedirect.com/science/article/pii/S1270963818319400

[3] J. Morgado, M. Abdollahzadeh, M. Silvestre, J. Páscoa, High altitude propeller design and analysis, Aerospace Science and Technology 45 (2015) 398 – 407. doi:https://doi.org/10.1016/j.ast.2015.06.011. URL http://www.sciencedirect.com/science/article/pii/S1270963815001881

[4] H. Du, J. Li, W. Zhu, Z. Qu, L. Zhang, M. Lv, Flight performance simulation and station-keeping endurance analysis for stratospheric super-pressure balloon in real wind field, Aerospace Science and Technology 86 (2019) 1 – 10. doi:https://doi.org/10.1016/j.ast.2019.01.001. URL http://www.sciencedirect.com/science/article/pii/S1270963818313312

[5] L. Delle Monache, S. Candido, A. Singh, Lower-stratosphere wind predictions with an analog ensemble, in: AGU Fall Meeting Abstracts, 2018.

[6] T. Désert, T. Jardin, H. Bézard, J. Moschetta, Numerical predictions of low reynolds number compressible aerodynamics, Aerospace Science and Technology 92 (2019) 211 – 223. doi:https://doi.org/10.1016/j.ast.2019.05.064. URL http://www.sciencedirect.com/science/article/pii/S1270963818327342

[7] G. Serino, T. Magin, P. Rambaud, F. Pinna, Statistical inverse analysis and stochastic modeling of transition, in: 43rd AIAA Fluid Dynamics Conference, 2013, p. 2883.

[8] L. A. Grzelak, J. A. S. Witteveen, M. Suárez-Taboada, C. W. Oosterlee, The stochastic collocation monte carlo sampler: highly efficient sampling from 'expensive' distributions, Quantitative Finance 19 (2) (2019) 339–356. arXiv:https://doi.org/10.1080/14697688.2018.1459807, doi:

10.1080/14697688.2018.1459807.
URL https://doi.org/10.1080/14697688.2018.1459807

[9] C. J. Geyer, On the convergence of monte carlo maximum likelihood calculations, Journal of the Royal Statistical Society: Series B (Methodological) 56 (1) (1994) 261–274.

[10] R. Pulch, Stochastic collocation and stochastic galerkin methods for linear differential algebraic equations, Journal of Computational and Applied Mathematics 262 (2014) 281 – 291, selected Papers from NUMDIFF-13. doi:https://doi.org/10.1016/j.cam.2013.10.046.
URL http://www.sciencedirect.com/science/article/pii/S0377042713005992

[11] D. Xiu, G. E. Karniadakis, Modeling uncertainty in flow simulations via generalized polynomial chaos, Journal of computational physics 187 (1) (2003) 137–167.

[12] M. A. Patterson, A. V. Rao, Exploiting sparsity in direct collocation pseudospectral methods for solving optimal control problems, Journal of Spacecraft and Rockets 49 (2) (2012) 354–377. arXiv:https://doi.org/10.2514/1.A32071, doi:10.2514/1.A32071.
URL https://doi.org/10.2514/1.A32071

[13] J. Mockus, Application of bayesian approach to numerical methods of global and stochastic optimization, Journal of Global Optimization 4 (4) (1994) 347–365.

[14] H. Tiesler, R. M. Kirby, D. Xiu, T. Preusser, Stochastic collocation for optimal control problems with stochastic pde constraints, SIAM Journal on Control and Optimization 50 (5) (2012) 2659–2682.

[15] G. H. Golub, J. H. Welsch, Calculation of gauss quadrature rules, Mathematics of computation 23 (106) (1969) 221–230.

[16] W. Gautschi, Construction of gauss-christoffel quadrature formulas, Mathematics of Computation 22 (102) (1968) 251–270.

[17] J. Feinberg, H. P. Langtangen, Chaospy: An open source tool for designing methods of uncertainty quantification, Journal of Computational Science 11 (2015) 46–57.

[18] G. Tang, G. Iaccarino, Subsampled gauss quadrature nodes for estimating polynomial chaos expansions, SIAM/ASA Journal on Uncertainty Quantification 2 (1) (2014) 423–443.

[19] J. Waldvogel, Fast construction of the fejér and clenshaw–curtis quadrature rules, BIT Numerical Mathematics 46 (1) (2006) 195–202.

[20] R. Madankan, P. Singla, A. Patra, M. Bursik, J. Dehn, M. Jones, M. Pavolonis, B. Pitman, T. Singh, P. Webley, Polynomial chaos quadrature-based minimum variance approach for source parameters estimation, Procedia Computer Science 9 (2012) 1129 – 1138, proceedings of the International Conference on Computational Science, ICCS 2012. doi:https://doi.org/10.1016/j.procs.2012.04.122.
URL http://www.sciencedirect.com/science/article/pii/S1877050912002438

[21] J. Son, Y. Du, Comparison of intrusive and nonintrusive polynomial chaos expansion-based approaches for high dimensional parametric uncertainty quantification and propagation, Computers and Chemical Engineering 134 (2020) 106685. doi:https://doi.org/10.1016/j.compchemeng.2019.106685.
URL http://www.sciencedirect.com/science/article/pii/S0098135419310026

[22] G. Onorato, G. Loeven, G. Ghorbaniasl, H. Bijl, C. Lacor, Comparison of intrusive and non-intrusive polynomial chaos methods for cfd applications in aeronautics, in: V European Conference on Computational Fluid Dynamics ECCOMAS, Lisbon, Portugal, 2010, pp. 14–17.

[23] A. Gel, R. Garg, C. Tong, M. Shahnam, C. Guenther, Applying uncertainty quantification to multiphase flow computational fluid dynamics, Powder Technology 242 (2013) 27 – 39, selected Papers from the 2010 NETL Multiphase Flow Workshop. doi:https://doi.org/10.1016/j.powtec.2013.01.045.
URL http://www.sciencedirect.com/science/article/pii/S0032591013000739

[24] J. Gonzalo, D. López, D. Domínguez, A. García, A. Escapa, On the capabilities and limitations of high altitude pseudo-satellites, Progress in Aerospace Sciences 98 (2018) 37–56. doi:10.1016/j.paerosci.2018.03.006.
URL https://doi.org/10.1016%2Fj.paerosci.2018.03.006

[25] X. Liu, W. He, Performance calculation and design of stratospheric propeller, IEEE Access 5 (2017) 14358–14368. doi:10.1109/access.2017.2725303.
URL https://doi.org/10.1109%2Faccess.2017.2725303

[26] J. Morgado, R. Vizinho, M. Silvestre, J. Páscoa, XFOIL vs CFD performance predictions for high lift low reynolds number airfoils, Aerospace Science and Technology 52 (2016) 207–214. doi:10.1016/j.ast.2016.02.031.
URL https://doi.org/10.1016%2Fj.ast.2016.02.031

[27] R. MacNeill, D. Verstraete, Blade element momentum theory extended to model low reynolds number propeller performance, The Aeronautical Journal 121 (1240) (2017) 835–857. doi:10.1017/aer.2017.32.
URL https://doi.org/10.1017%2Faer.2017.32

[28] J. Jiao, B.-F. Song, Y.-G. Zhang, Y.-B. Li, Optimal design and experiment of propellers for high altitude airship, Proceedings of the Institution of Mechanical Engineers, Part G: Journal of Aerospace Engineering 232 (10) (2018) 1887–1902. arXiv:https://doi.org/10.1177/

0954410017704217, doi:10.1177/0954410017704217.
URL https://doi.org/10.1177/0954410017704217

[29] H. S. Ribner, S. P. Foster, Ideal efficiency of propellers-theodorsen revisited, Journal of aircraft 27 (9) (1990) 810–819.

[30] Q. R. Wald, The aerodynamics of propellers, Progress in Aerospace Sciences 42 (2) (2006) 85–128. doi:10.1016/j.paerosci.2006.04.001.
URL https://doi.org/10.1016%2Fj.paerosci.2006.04.001

[31] S. Goldstein, On the vortex theory of screw propellers, Proceedings of the Royal Society of London. Series A, Containing Papers of a Mathematical and Physical Character 123 (792) (1929) 440–465.

[32] M. Drela, First-order dc electric motor model, Massachusetts Institute of Technology.

[33] A. Gong, R. MacNeill, D. Verstraete, Performance Testing and Modeling of a Brushless DC Motor, Electronic Speed Controller and Propeller for a Small UAV Application, 2018 Joint Propulsion Conference (2018) 1–15doi:10.2514/6.2018-4584.
URL https://arc.aiaa.org/doi/10.2514/6.2018-4584

[34] A. García-Gutiérrez, J. Gonzalo, D. Domínguez, D. López, A. Escapa, Aerodynamic optimization of propellers for high altitude pseudo-satellites, Aerospace Science and Technology 96 (2020) 105562. doi:https://doi.org/10.1016/j.ast.2019.105562.
URL http://www.sciencedirect.com/science/article/pii/S1270963819323375

[35] E. Kalnay, M. Kanamitsu, R. Kistler, W. Collins, D. Deaven, L. Gandin, M. Iredell, S. Saha, G. White, J. Woollen, Y. Zhu, M. Chelliah, W. Ebisuzaki, W. Higgins, J. Janowiak, K. C. Mo, C. Ropelewski, J. Wang, A. Leetmaa, R. Reynolds, R. Jenne, D. Joseph, The ncep/ncar 40-year reanalysis project, Bulletin of the American Meteorological Society 77 (3)

(1996) 437–472. arXiv:https://doi.org/10.1175/1520-0477(1996)077<0437:TNYRP>2.0.CO;2, doi:10.1175/1520-0477(1996)077<0437:TNYRP>2.0.CO;2.
URL https://doi.org/10.1175/1520-0477(1996)077<0437:TNYRP>2.0.CO;2

[36] P. V. Gamboa, M. A. R. Silvestre, Airfoil Optimization With Transition Curve As Objective Function, VI International Conference on Adaptive Modeling and Simulation ADMOS 2013 (June 2013) (2013) 1–12.

[37] K. Wang, Z. Zhou, X. Zhu, X. Xu, Aerodynamic design of multi-propeller/wing integration at low reynolds numbers, Aerospace Science and Technology 84 (2019) 1 – 17. doi:https://doi.org/10.1016/j.ast.2018.07.023.
URL http://www.sciencedirect.com/science/article/pii/S1270963817320060

[38] T. J. Mueller, L. J. Pohlen, P. E. Conigliaro, B. J. Jansen, The influence of free-stream disturbances on low Reynolds number airfoil experiments, Experiments in Fluids 1 (1) (1983) 3–14. doi:10.1007/BF00282261.

[39] J. F. Marchman, T. D. Werme, Clark-Y Airfoil Performance at Low Reynolds, AI AA-84-0052 Numbers AlAA 22nd Aerospace Sciences Meeting.

[40] J. Winslow, H. Otsuka, B. Govindarajan, I. Chopra, Basic Understanding of Airfoil Characteristics at Low Reynolds Numbers (104–105), Journal of Aircraft (2017) 1–12doi:10.2514/1.C034415.
URL https://arc.aiaa.org/doi/10.2514/1.C034415

[41] M. Caboni, E. Minisci, A. Riccardi, Aerodynamic design optimization of wind turbine airfoils under aleatory and epistemic uncertainty, 2018, the Science of Making Torque from Wind 2018, TORQUE 2018 ; Conference date: 20-06-2018 Through 22-06-2018.
URL http://www.torque2018.org/





Please cite this article in press as: García-Gutiérrez, A., Gonzalo, J., López, D., Delgado, A (2020). Stochastic design of high altitude propellers. *Aerospace Science and Technology*, 107, 106283, https://www.sciencedirect.com/science/article/pii/S1270963820309652

[42] M. Drela, Xfoil: An analysis and design system for low reynolds number airfoils, in: Low Reynolds number aerodynamics, Springer, 1989, pp. 1–12.

[43] L. Mack, Transition and laminar instability theory, JPL Publication (1956) 77–15.

[44] T. A. Shaw, Mises implementation of modified abu-ghannam / shaw transition criterion ( second revision ), 2008.

[45] J. Lumley, K. Takeuchi, Application of central-limit theorems to turbulence and higher-order spectra, Journal of Fluid Mechanics 74 (3) (1976) 433–468.

[46] J. G. Coder, M. D. Maughmer, Computational fluid dynamics compatible transition modeling using an amplification factor transport equation, AIAA Journal 52 (11) (2014) 2506–2512. `arXiv:https://doi.org/10.2514/1.J052905`, `doi:10.2514/1.J052905`.
URL `https://doi.org/10.2514/1.J052905`

[47] M. Simons, Model Aircraft Aerodynamics (1994).

[48] E. J.N, A. Sherman, Airfoil Section Characteristics as Affected by Variations of the Reynold's Number, NACA Report 586.

[49] K. Koca, M. S. Genç, H. H. Açıkel, M. Çağdaş, T. M. Bodur, Identification of flow phenomena over NACA 4412 wind turbine airfoil at low Reynolds numbers and role of laminar separation bubble on flow evolution, Energy 144 (2018) 750–764. `doi:10.1016/j.energy.2017.12.045`.

[50] P. Lissaman, Low-reynolds-number airfoils, Annual review of fluid mechanics 15 (1) (1983) 223–239.

[51] R. MacNeill, D. Verstraete, A. Gong, Optimisation of Propellers for UAV Powertrains. `arXiv:https://arc.aiaa.org/doi/pdf/10.2514/6.2017-5090`, `doi:10.2514/6.2017-5090`.
URL `https://arc.aiaa.org/doi/abs/10.2514/6.2017-5090`





Please cite this article in press as: García-Gutiérrez, A., Gonzalo, J., López, D., Delgado, A (2020). Stochastic design of high altitude propellers. *Aerospace Science and Technology*, 107, 106283, https://www.sciencedirect.com/science/article/pii/S1270963820309652

[52] E. Peponakis, A. Paspatis, R. Oikonomidis, G. Barzegkar-Ntovom, K. Bampouras, A simple low cost setup for thrust and energy efficiency calculation for small brushless dc motors, ECESCON 9 85–89.

[53] P. Bogusz, M. Korkosz, J. Prokop, A study of design process of bldc motor for aircraft hybrid drive, in: 2011 IEEE International Symposium on Industrial Electronics, 2011, pp. 508–513.

[54] Z. Zheng, W. Huo, Z. Wu, Trajectory tracking control for underactuated stratospheric airship, Advances in Space Research 50 (7) (2012) 906–917.

[55] W. Gautschi, Gauss–radau formulae for jacobi and laguerre weight functions, Mathematics and Computers in Simulation 54 (4-5) (2000) 403–412.

[56] X. Du, L. Leifsson, Optimum aerodynamic shape design under uncertainty by utility theory and metamodeling, Aerospace Science and Technology 95 (2019) 105464. doi:https://doi.org/10.1016/j.ast.2019.105464. URL http://www.sciencedirect.com/science/article/pii/S127096381930570X

[57] F. Wang, S. Yang, F. Xiong, Q. Lin, J. Song, Robust trajectory optimization using polynomial chaos and convex optimization, Aerospace Science and Technology 92 (2019) 314 – 325. doi:https://doi.org/10.1016/j.ast.2019.06.011. URL http://www.sciencedirect.com/science/article/pii/S1270963818316444

[58] L. Zhang, J. Li, Y. Jiang, H. Du, W. Zhu, M. Lv, Stratospheric airship endurance strategy analysis based on energy optimization, Aerospace Science and Technology 100 (2020) 105794. doi:https://doi.org/10.1016/j.ast.2020.105794. URL http://www.sciencedirect.com/science/article/pii/S1270963819326872





Please cite this article in press as: García-Gutiérrez, A., Gonzalo, J., López, D., Delgado, A (2020). Stochastic design of high altitude propellers. *Aerospace Science and Technology*, 107, 106283, https://www.sciencedirect.com/science/article/pii/S1270963820309652